NRIAG Journal of Astronomy and Geophysics (2016) 5, 403–412

National Research Institute of Astronomy and Geophysics

NRIAG Journal of Astronomy and Geophysics

www.elsevier.com/locate/nrjag

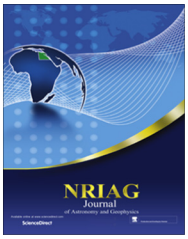

Mapping *b*-values beneath Abu Dabbab from June to August 2004 earthquake swarm

I.F. Abu El-Nader [a,b,*], **A. Shater** [b], **H.M. Hussein** [a,b]

[a] *National Research Institute of Astronomy and Geophysics, Seismology Department, Helwan, Egypt*
[b] *North Africa Seismological Group for Earthquakes and Tsunami Studies NAGET, Net40 OEA ICTP, Italy*

Received 26 May 2016; revised 18 July 2016; accepted 18 July 2016
Available online 28 September 2016

KEYWORDS

Abu Dabbab;
swarm;
b-value

Abstract Abu Dabbab area is considered as one of the most active earthquake sources in Egypt. It is defined by its swarm type activity, and complicated stress pattern. This study was conducted to evaluate the two and three dimensional spatial distribution of *b*-value at Abu Dabbab area (Margin of the northern Red Sea Rift, Egypt). The gridding technique of Wiemer and Wyss (1997) was used to compute *b*-value using ZMAP software. The *b*-value is calculated from a catalog consisting of 850 well-located earthquakes, which were recorded from 1st June to August 2004, using the maximum likelihood method. These earthquakes were recorded by temporary digital seismic network, with magnitudes ranging from −1 to 3.4 ML. It is important to mention that the variations of *b*-value with time cannot be easily detected for a short period. Hence, this study has been carried out to examine the variations of *b-value* in space. The computed *b*-value in the Abu Dabbab area does not follow a uniform distribution. A small volume of anomalously high *b*-value ($b > 1.8$) exists in the central part of the area at a depth between 6 and 9 km. This seems to agree with the reported low velocity value derived from previous P-wave travel time tomography studies (Hosny et al., 2009) and the low *Q* value (Abdel-Fattah et al., 2008). The existence of an anomalously high *b*-value region may be attributed to the presence of a magma reservoir or dyke zone beneath the northern Red Sea Rift that causes an intensively heterogeneous fractured crust or unusually high pore pressure.

* Corresponding author at: National Research Institute of Astronomy and Geophysics, Seismology Department, Helwan, Egypt.
E-mail addresses: ememan70@yahoo.com, hesham6511421@yahoo.com (I.F. Abu El-Nader).

Peer review under responsibility of National Research Institute of Astronomy and Geophysics.

Production and hosting by Elsevier

1. Introduction

"Abu Dabbab" is located in the Eastern Desert of Egypt, 24 km from the Red Sea shoreline, and is considered as one of the most active earthquake sources in Egypt (Fig. 1). Recent studies (e.g., El-Hady, 1993; Ibrahim and Yokoyama, 1994) showed that Abu Dabbab region is characterized by a fairly continuous seismic activity. The earthquakes of the 12th November, 1955, (*mb* = 6.1) and the 2nd June, 1984

http://dx.doi.org/10.1016/j.nrjag.2016.07.002

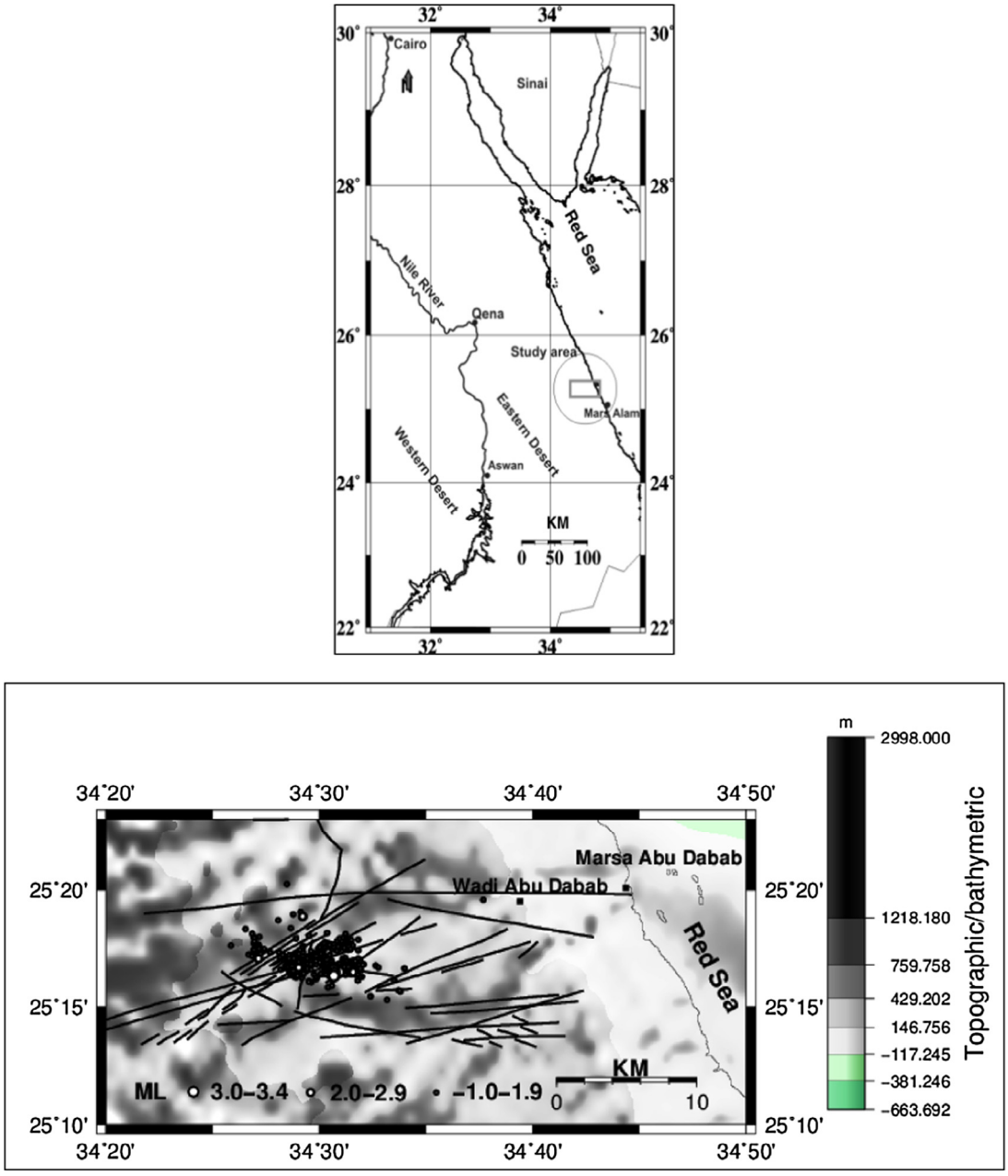

Figure 1 Map view shows the regional location of the study area marked by gray square (top), at bottom a map showing the spatial distribution of the June–August 2004 earthquake swarms together with the surface faults passing through the Abu Dabbab area (modified after Akawy, 2008).

(*mb* = 5.1), were occurred in this area. The area is commonly well characterized by intense micro-earthquake activity associated with 'sounds' periodically occurring as swarms (Morgan et al., 1981). Those sounds are produced by distinct rumbling, which is similar to the sound of distant blast. The historical reports revealed that these 'peculiar' sounds have been heard by the tribes accompanied this land from many years ago. Furthermore, the Arabic name of "Abu Dabbab" is driven from this unique sound phenomenon ('Dabbab' is hammering sound).

Several earthquake swarms (e.g., swarms of 1976, 1984, and 1993) have been recorded and discussed by several authors (Hamada 1968; Fairhead and Girdler, 1970; Daggett and Morgan, 1977; Daggett et al., 1986; El-Hady, 1993; Ibrahim and Yokoyama, 1994; Badawy et al., 2008). Recently, some swarms have been recorded in January 2003, October 2003, and the period between July and August 2004.

It has been suggested that the occurrence of earthquakes at a certain seismic sequence is due to stress perturbations associated with the migration of magmatic or hydrothermal fluids through new or pre-existing crustal heterogeneities including crustal fractures (Hill, 1977; Toda et al., 2002; Waite and Smith, 2002), aseismic slip or fluid pressure differences (Vidale et al., 2006). In controversy with most of the studies conducted on Abu Dabbab area, the outcome of the study by Daggett et al. (1986) attributed such swarms to a plutonic

intrusion (igneous activity) within the Precambrian crust, rather than regional tectonic. Moreover, the evidences of high heat flows revealed that the high level of seismic activity of Abu Dabbab is probably due to igneous activity. The heat flows at Abu Dabbab is twice the average value of the Eastern Desert (47 mW/m^2) (Mogi, 1962). The brittle-ductile transition boundary at Abu Dabbab area is found at a relatively shallow depth (9–10 km) as deduced from the depth distribution of the earthquakes and the rheological studies (El Hady, 1993). This implies a shallow athenospheric intrusion anomaly.

The data set recorded from June to August 2004 swarms has been previously utilized in the research works by Mohamed, 2005; Hosney et al., 2009; Hussein et al., 2011. They concluded that the seismic activity appears to be more or less concentrated and clustered at the intersection zones of faults. Clusters show strike slip, oblique slip, reverse and normal faults movement in the upper crust. These faults appear to follow two main active fault trends. The first belongs to a normal fault system (NW-SE) parallel to the Red Sea while the other set is a transverse one, perpendicular to the Red Sea margin. The majority of seismic events are abundant at depths of 5–8 km and 10–13 km, respectively. The results of Hussein et al. (2008) agreed with the assumption that the hypocentral migration at Abu Dabbab is mainly related to intruded dyke.

The aim of this study was to map the *b-value* from the earthquake swarms occurred during June–August 2004. This study was designed to calculate the spatial distribution of *b*-value in order to understand Abu Dabbab's swarms and compare these results with the *Vp*/*Vs* ratio and *P*- and *S*-velocity tomographic inversion performed using the same earthquakes. The average *b*-value for most tectonic regions of the earth is approximately ($b \sim 1$) (Minakami, 1990). Conversely, in the volcanic areas, most of the crust shows usual value or even low *b*-value with rather small volumes of anomalously high *b*-value ($b > 1.3$) (Wyss and Wiemer, 1997; Wiemer and McNutt, 1997). There are several factors responsible for the high *b*-value anomalies such as: a high material heterogeneity (Mogi, 1962), low applied stress (Scholz, 1968), high thermal gradient (Warren and Latham, 1970), or low effective stress (high pore pressures) (Wyss, 1973).

The relative number of small to large earthquakes that occurred in a given area at a certain time is referred to as "*b*-value". This value can be calculated from the following equations (Ishimoto and Iida, 1939; Gutenberg and Richter, 1944):

$$\log_{10} N = a - bM \tag{1}$$

where N is the cumulative number of earthquakes having magnitudes equal to or larger than M, and $a$and b are constants related to the activity and earthquake size distribution, respectively. The coefficient b describes the slope of the frequency-magnitude distribution of earthquakes FMD. To estimate the *b*-value, a maximum likelihood method is the most commonly used (Aki, 1965; Bender, 1983; Utsu, 1999):

$$b = \frac{\log_{10}(e)}{[(M) - (Mc - dM_{bin}/2)]} \tag{2}$$

where M is the mean magnitude of the sample and ∂M_{bin} is the binning width of the data set.

The present analysis requires accurate hypocenter location as well as a complete data set. It is frequently necessary to use the maximum number of events available for high quality studies (Wiemer and Wyss, 2000). This means that an increase in the number of earthquakes will enhance the resolution of the results.

2. Tectonic setting

Abu Dabbab area is defined by a complicated structure pattern. The corresponding whole rock sequence which includes basement rocks, Neogene sediments and Quaternary alluvial deposits is deformed by four main faults and fracture trends in the N-S, NE-SW, NW-SE and E-W directions with different types and senses of motion (Fig. 1). On the basis of analyzing the fault scarps, drainage pattern, and field data measurements, Aqaway (2008) fully described the history of initiation and reactivation of these fault trends. He concluded that there is a relation between the current Red Sea tectonics and the activity of these faults. The regional and local extensional stresses are combined causing reactivation and/or neoformation of all fault trends in the study area. The present active drainages are also affected by the existing four trends of the main faults. A fault segmentation phenomenon is common for all fault trends which means that the faults are still growing and coalesce during repeated local earthquakes (Gillespie et al., 1992; Davis et al., 2005).

Furthermore, the field study indicated that the N-S and E-W faults are more active than other trends. The E-W faults are considered as the most active one in the study area. El Gaby et al. (1988) named this trend as Sheikh Salam trend that mainly relates the Precambrian ENE to NE compressive stress. The E-W fault trend was recognized as right lateral strike slip faults (the older generation) and normal faults (the younger set) (Bosworth and Stecker, 1997). This tectonic trend runs for long distances across the Eastern Desert, passing through the Nile Valley into the Western Desert. Additionally, the N-S tectonic trend was recorded in the study area as normal faults, extensional fractures, and strike slip faults. Oblique mechanisms nature was also identified. Some N-S fractures are open and barren implying recent activation (Akawy, 2008). The Miocene rocks and the overlying Quaternary sediments are highly deformed by the N-S trending normal faults. The NE-SW fault trends are found as strike slip faults (right and left lateral), normal faults and extensional fractures which cut the Quaternary sediments section.

The inferred present day stress field from recent structural features, recent drainage modification and seismic data shows N-S compression and multi-directions of extension. The compression is due to the N to NW drift of Africa. The NE-SW extension across the Red Sea and the N to NW drift of Africa toward the European plate are the main reasons of the present stresses (Akawy, 2008).

3. Data

The epicenters of earthquakes used in this study at Abu Dabbab area (Mohamed, 2005) are shown in Fig. 2. A catalog composed of 850 events with local magnitude ranging from −1 to 3.6 is used in this study. The range of focal depth for these

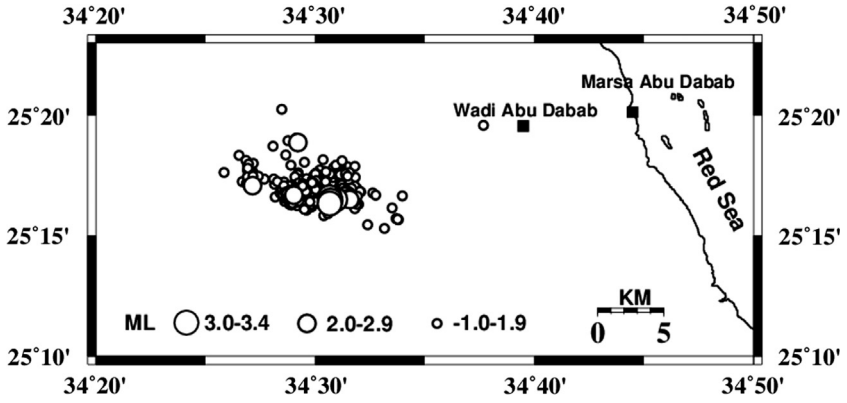

Figure 2 The spatial distribution of the epicenters of the June–August 2004 earthquake swarms.

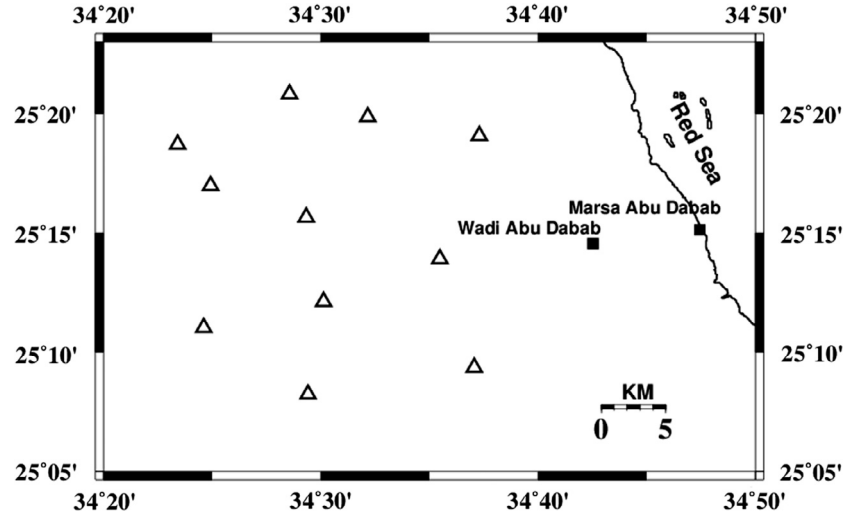

Figure 3 Location map of the portable stations distribution that used for monitoring earthquake activity at Abu Dabbab area during the period from 1 June 2004 to 20 August 2004.

events is between 3 and 15 km. The earthquake activity was monitored by a local network of eleven portable stations (Fig. 3) during the period from 1 June 2004 to 20 August 2004. This period of time offers more enough events for mapping the *b*-value at Abu Dabbab area in an attempt to understand the seismotectonic characteristics of this seismic zone. In fact, the available single permanent station in Abu Dabbab (ADB) region is not sufficient to locate the microearthquake activity in order to calculate the *b-value* and to investigate its spatial variation. Figs. 4a, b and 5b illustrate respectively the magnitude of events versus time, map of depth view of data set and a resolution map showing the maximum radius of the investigated area and the distribution of epicenters from which we select gridding space of samples. Using the 1-D velocity structure obtained from P-wave travel times (Marzouk, 1988), Hussein et al. (2008) relocated all earthquakes used in this study. The estimated location accuracies of these events are less than 0.3 km in both horizontal distance and depth. The earthquake swarms of June–August 2004 were concentrated at focal depths of 8–10 km and 11–15 km respectively. The majority of events occur between 9 and 10 km depth (Hussein et al., 2011).

4. Method

In this study, the spatial distribution of *b*-value is computed using the ZMAP software of Wiemer (2001), where the maximum likelihood method is applied. This method yields a more robust estimate than least square regression method (Aki, 1965; Hamilton, 1967). The first step of analyzing the *b*-values is determining the magnitude of completeness *Mc* and its uncertainty. *Mc* is defined as the lowest magnitude at which 100% of the events in a space and time are detected (Wiemer and Wyss, 2000). In other words, values below *Mc* are considered heterogeneous and incomplete. In this study *Mc* for Abu Dabbab data set was analyzed using the following sequence: at first *b* and *a* values of the Gutenberg-Richter (GR) power law using these four methods were estimated, and maximum curvature method, the goodness of fit test and the *Mc* by *b*-value stability (Cao and Gao, 2002).

The results appeared similar and do not differ greatly. In the present study the maximum curvature (MAXC) method described by Wyss et al. (1999) and Wiemer and Wyss (2000) was used to evaluate *Mc* due to its reliability and simplicity. The MAXC technique is a fast and simple way to estimate

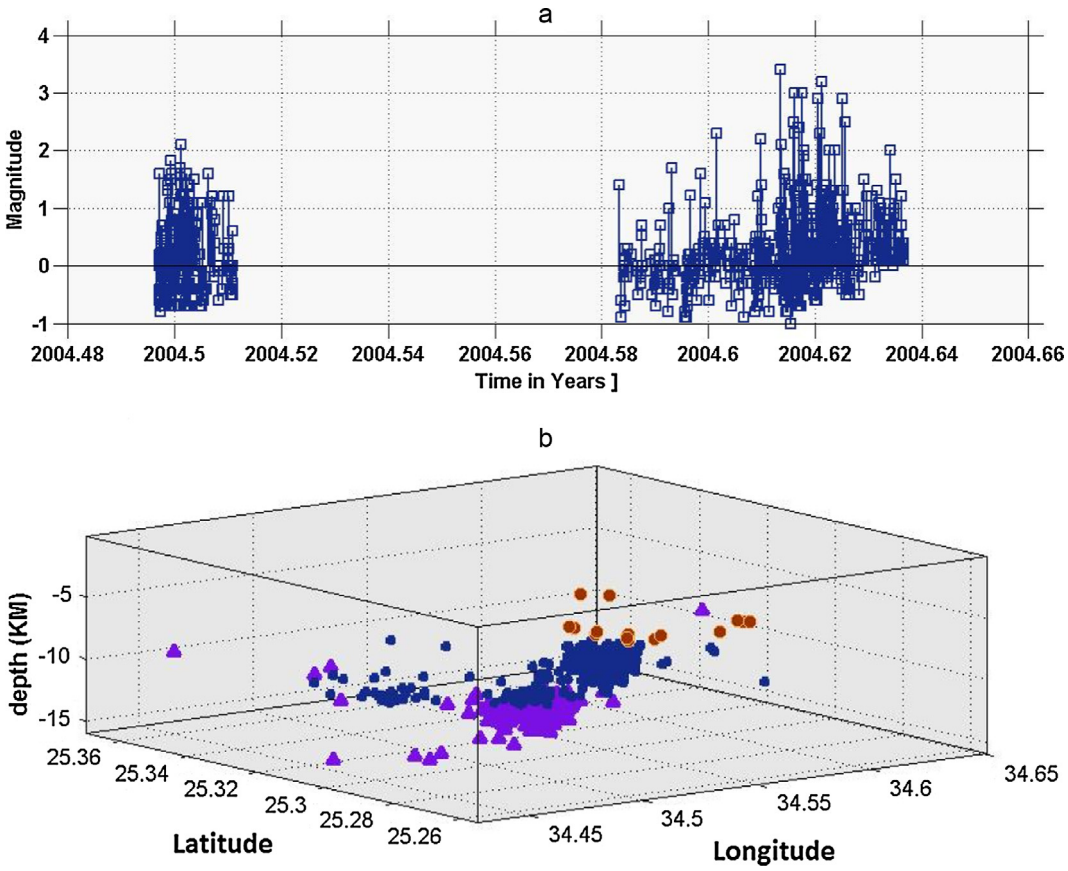

Figure 4 (a) Plot of magnitude of located events as a function of time and (b) view map of events as a function of depth.

Mc which is based on calculation of the magnitude bin with the highest frequency of events in the frequency magnitude plot. Fig. 5a shows the estimated *Mc* equal to 0.0. Then the synthetic distribution of magnitudes with the same *b*, *a*, and *Mc* values was computed as shown in Fig. 5b. Regarding mapping *Mc*, the gridding technique of Wiemer and Wyss (1997) was used. *Mc* must be estimated for each sample processed by the algorithm which is outlined in next section. This was due to the susceptibility of *Mc* changing with different depth and location. The *Mc* must be computed by estimation of the maximum value of the derivative of the frequency magnitude distribution (FMD). At the same time, a map of the goodness of fit test to a power law of GR in percentage was computed (Fig. 6a).

It is important to mention that the variations of *b*-value with time cannot be easily detected. By constructing differential *b*-value map for this short period between June and August 2004, the time factor has no significant effect on the *b*-value. Hence, this study has been carried out to examine the variations of *b-value* in space.

To map *b-value*, the method by Wiemer and Wyss (1997) and Wiemer and Katsumata (1999) was used. The *b*-value was computed in two and three dimensional grids with nodal points separated 0.002° horizontally and 0.002° vertically using a fixed number of earthquakes ($n = 50$) considering the nearest N events at each node of the grid taking into account the magnitude of completeness of the data as well. These parameter settings were selected as the best fit of the size of the area to be covered (Fig. 6b), density of earthquakes and the reliability of results. Many iterations are made for different grid spacing (i.e., 0.001–0.005°) as well as the number of events per sample has been changed from 10 to 70 events for detecting more stability of results. By using this grid method the radius varies with the earthquake density while the number of events is fixed. Furthermore we reestimate *b-value* by using another approach in which the radius was fixed and not the number of events at each node. The *b-value* was computed at different radii (i.e., at 1, 2, 3, 4, 5, 6, and 7 km) respectively to find the appropriate radius for resolving *b*-value contrasts in the area of study. It has been noticed that sampling with radii from 1 to 4 km shows essentially the same pattern but with different coverage. The radii values less than 3 km showed more details in *b*-value contrast. Thus the optimal radius for sampling events to map *b*-value is ranged from 1 to 3 km. The *b*-value is computed by using only the earthquakes with $M \geqslant Mc$. This technique requires that the number of earthquakes with $M \geqslant Mc$ must be larger than or equal to the minimum number of events located in each cell. Otherwise the *b*-value was discarded. Finally, the *b*-value estimated at each node is translated into a color code. Thus, we can identify the anomalous area of *b*-value.

The standard error of these *b*-values is given by Shi and Bolt (1982) as follows:

$$\sigma(b) = 2.30b^2\sqrt{(\Sigma_i(M_i - M_{mean})^2/n(n-1))} \quad (3)$$

where *n* is the total number of events of the given sample.

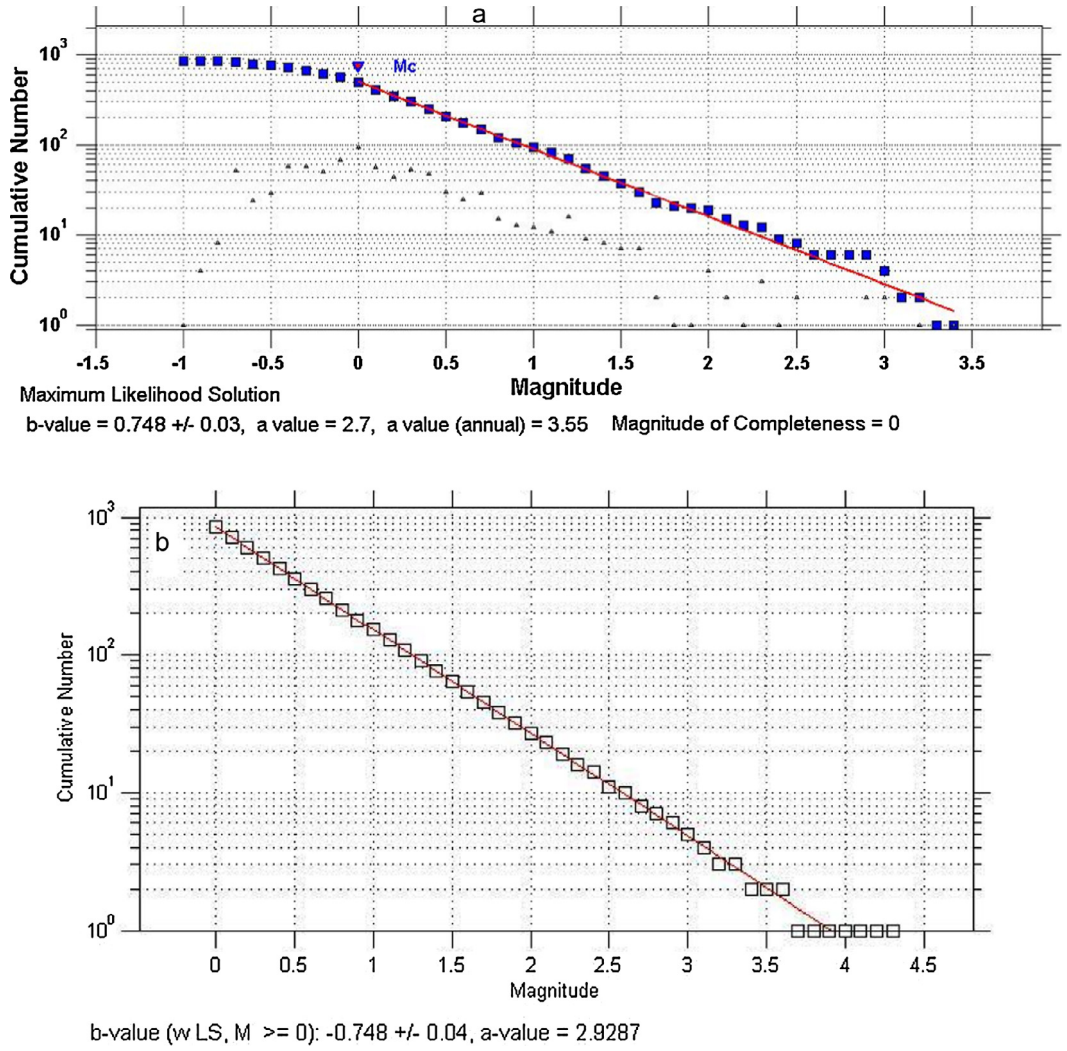

Figure 5 (a) Plot of observed cumulative number of events with magnitude and (b) plot of synthetic frequency magnitude distribution (FMD).

The difference between two *b*-values is considered significant if they are different either at 95% confidence interval or higher. However, $\sigma(b)$ seems to underestimate the true standard deviation of *b*-value based on the assumption of complete catalog and a correct estimation of the magnitude of completeness *Mc*. Therefore, we compute the standard deviation of *b*-value using the boot strap approach, taking into consideration the *Mc* standard error as described by Schorlemmer et al. (2003).

5. Results

The combination of the relatively high seismicity, swarm type activity, and the complicated stress pattern of Abu Dabbab area suggests that the spatial changes of *b*-values may be considered as an important characteristic of this area, providing additional insights for the cause of earthquake swarms. Fig. 6c illustrates the map of the magnitude of the completeness value computed for the earthquake swarm of June–August 2004. The magnitude of completeness changes spatially between −0.6 and 0.4. However, there is one value for each node which is the minimum magnitude above which this node is complete. The minimum threshold magnitude ($Mc = 0$; Fig. 5a) for all grid points is also selected automatically by the ZMAP software. Thus, the analysis is restricted only to earthquakes of $M \geqslant Mc$. To assess the validity of our calculations, we determined the standard errors.

The resulting spatial distribution of *b*-value in Abu Dabbab area revealed areas of high and low values as well as areas of normal crustal values as demonstrated in the two-dimensional map (Fig. 7a). The *b*-value ranges between 0.5 and 1.8. The majority of errors in *b*-value are less than 0.1 (Fig. 7b). Fig. 7c displays a plot of *b*-value as a function of depth for earthquakes in the study area. The two dimensional map does not reflect a clear picture while the cross section shown in Fig. 8 as well as the three dimensional one in Fig. 9 show clear pictures for the distribution of the *b*-values with depth. On the cross section (Fig. 8) one can see that the high *b*-value extends from 4 to 10 km depth. It displays two high *b*-value areas stand out, one extending from 7 to 9 km depth, while the other one exists at 11 km depth. Mapping of *b*-value in three dimensions (Fig. 9), shows anomalously

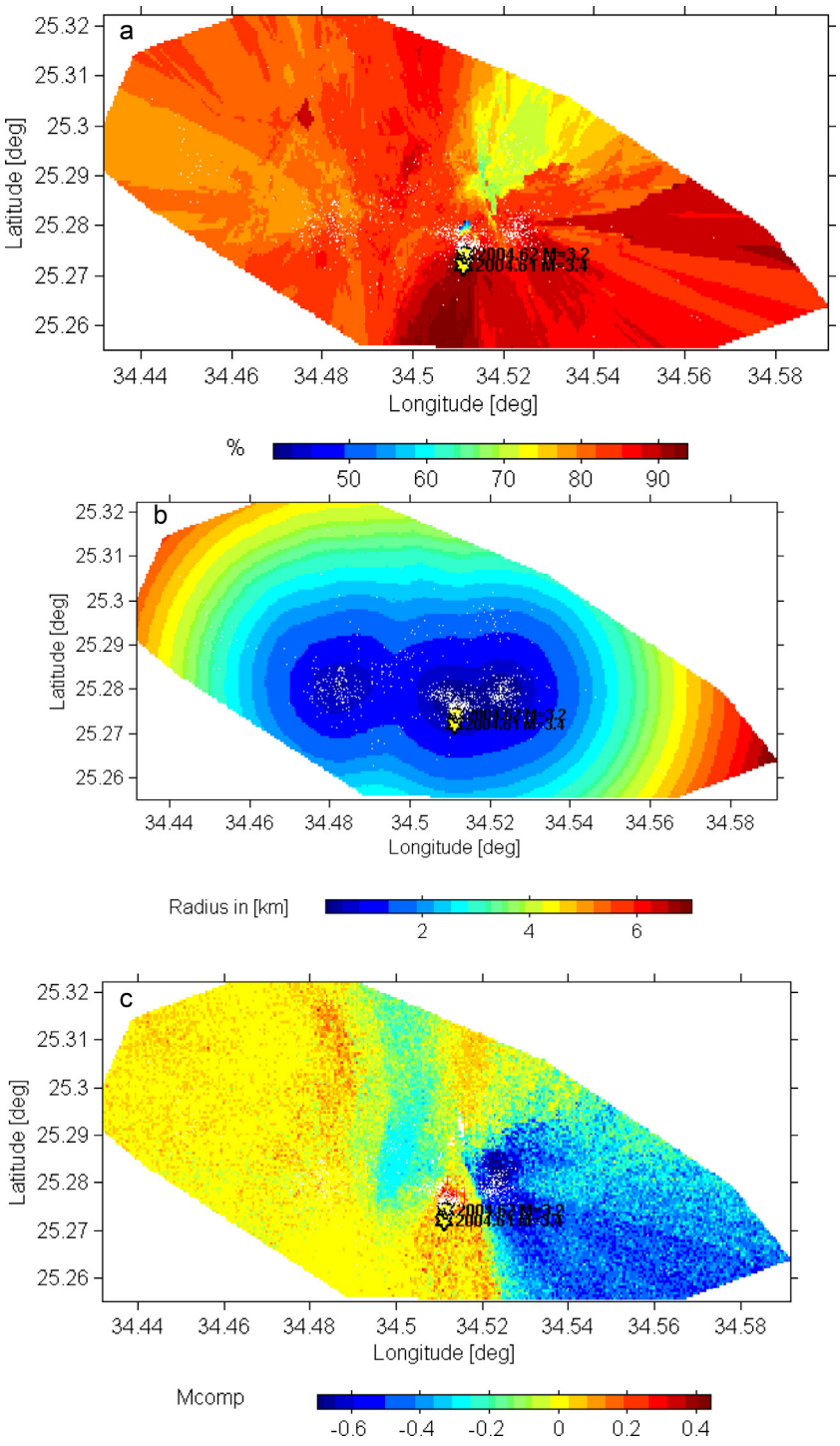

Figure 6 (a) Map of the goodness of fit of a straight line to the observed frequency magnitude relation in percent of the data modeled correctly; (b) image of the radius range computed by ZMAP software; and (c) image of the range of threshold magnitude for all grid point values, *Mc* (Magnitude of completeness) as computed by ZMAP software.

higher *b*-value ($b \sim 1.8$) in the central part of the area above 9 km depth. This high value was concentrated in small volume while the surrounding crust beneath Abu Dabbab shows normal to low values. This is clearly appearing in the cross section (Fig. 8). This depth is the same depth where the *mb* 5.1 earthquake of 1984 occurred. This event displays a high stress drop of 9.7 MPa and strike slip faulting mechanism with normal component (Hussein et al., 2011). This depth also represents the depth of the brittle-ductile transition zone (El Hady, 1993), where the maximum shear stress exists. An intensive activity is found at this depth which indicates a more heterogeneous medium with numerous small fractures (Hussein et al., 2011). This is being consistent with the relatively high heat flow (92 mW/m^2) in Abu Dabbab area which is mainly attributed to

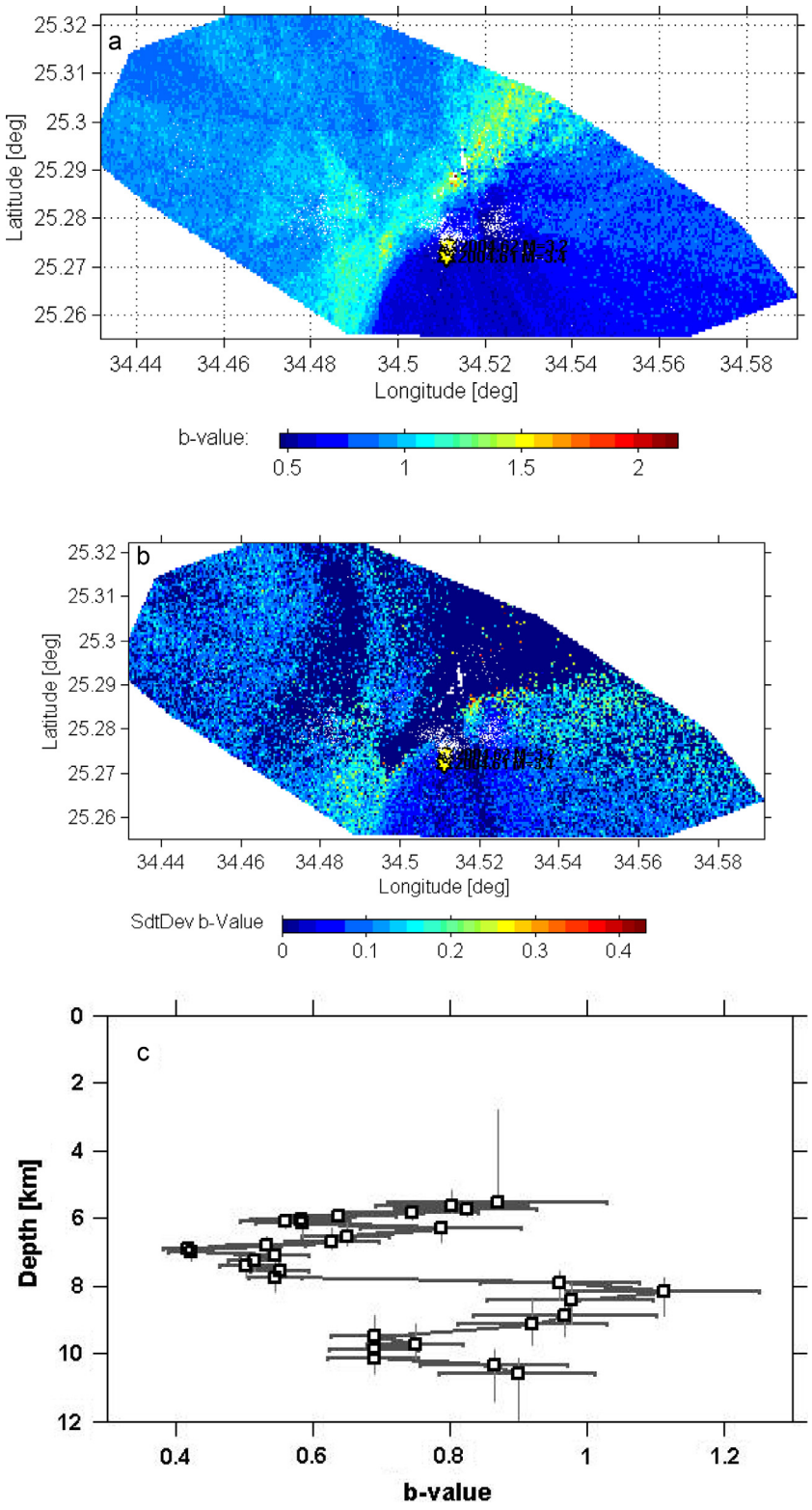

Figure 7 (a) Two-dimensional image of the *b*-values distribution, grid spacing is 0.002°, *b*-value at each node was determined using the maximum likelihood method; (b) standard deviation; and (c) average *b-value* versus depth for earthquakes in Abu Dabbab area, each point represents 50 events with overlap of 5 events, horizontal bars are standard deviations of *b*-value, and vertical bars are the depth that is represented by overlapped events.

the emplacement of magmatic fluids. Furthermore, the anomalously high *b*-value in the depth range of 6–9 km coincides well with the low P-wave velocity anomaly and high Vp/Vs ratio deduced from tomographic studies (Hosny et al., 2009) and low Q value (Abdel Fattah et al., 2008) as well. Hoseny et al. (2011) showed that the earthquakes occurring at a depth

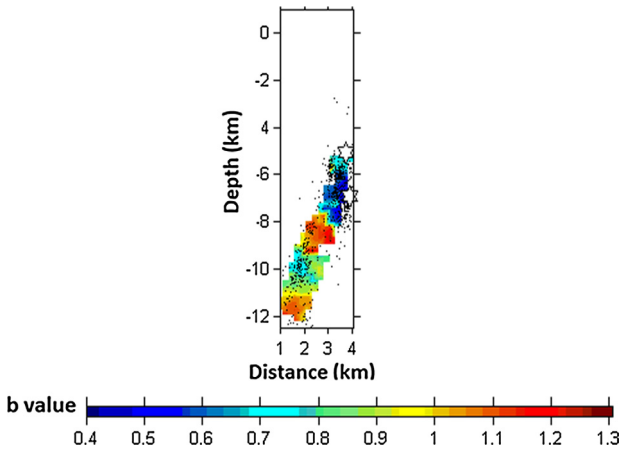

Figure 8 Cross section through the investigated area, to compute *b*-value and a grid spacing of 0.2 km horizontally and 0.2 km vertically was used.

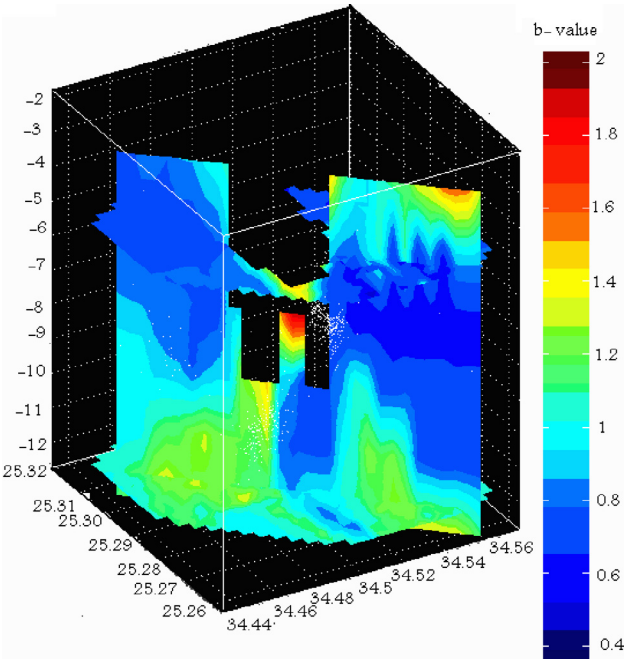

Figure 9 Plot of *b*-value in three dimensions, the separation of nodes is 0.002° (latitude/longitude), and 1 km for depth, the number of earthquakes used for estimating *b*-value is kept constant at $N_{min} = 50$.

of less than 9 km reflect high compensated linear vector dipole (CLVD) ratio. The resulting focal mechanism solutions of some events at this depth range indicate reverse faulting mechanism in contrary to suggestion of Schorlemmer et al. (2005) that high, medium, and low *b*-values correlate worldwide with normal, strike-slip and thrust faulting respectively. The composite fault plane solution obtained from the P-wave first motion of the micro-earthquakes which lie in the depth range of 8–10 km shows a reverse faulting mechanism (Hussein et al., 2011). The observed reverse slip in Abu Dabbab may be attributed to magma intrusion. Khodayar and Einarsson (2004) suggest that dyke intrusions are one of the kinematic origins for the observed reverse faulting mechanisms.

6. Discussion and conclusions

We interpret the anomalously high *b*-value at depths 6–9 km beneath Abu Dabbab as a result of the presence of active shallow magma reservoir beneath the northern Red Sea Rift which facilitates the formation of concentrated dyke since Abu Dabbab area is located very close to the margin of the northern Red Sea Rift where the crustal thickness varied from 5.1 to 8.3 km throughout the main trough (Gaulier et al., 1988a). All evidences support the idea that this seismic activity at Abu Dabbab area is due to this reservoir which is the starting point of intrusion. The presence of magma chamber gives rise to the main factors linked with the high heterogeneity, high pore pressure and high thermal gradient. On other words, the high *b*-values are considered as indication of high crustal heterogeneity of the local stress regime (Farrell et al., 2009). This high heterogeneity of stress causes numerous small cracks in the crust to be oriented in all directions. The existence of linear trend of small earthquakes extending from the axis of the Red Sea toward Abu Dabbab supports our conclusion. This band of seismicity coincides with one of the accommodation zones existing in the northern Red Sea.

It is clear that the insufficient coverage of the recording stations of the Egyptian National Seismological Network at Abu Dabbab area limited the continuous observation of the seismic activity. However, the present analysis requires a long-term observation of the seismic activity at Abu Dabbab. Therefore, there is a necessity for installing permanent local seismological network for obtaining the location of microearthquakes with higher accuracy for future studies concerning this area.

The *b-value* computed in this study is found to range between 0.5 and 1.8. A high *b-value* anomaly was detected at a depth below 7. This is due to the migration of fluids from a magma storage in the Red Sea along the accommodation zones which passes through Abu Dabbab area. The low P-wave velocity anomaly and high *Vp*/*Vs* ratio deduced from tomographic studies (Hosny et al., 2009; Shater, personal communication) and low *Q* value (Abdel Fattah et al., 2008) at this depth supports this interpretation.

References

Abdel-Fattah, A.K., Morsy, M., El Hady, S., Kim, K.Y., Sami, M., 2008. Intrinsic and scattering attenuation in the crust of the Abu Dabbab area in the Eastern Desert of Egypt. Phys. Earth Planet. Inter. 168, 103–112.

Akawy, A., 2008. Exhumed and Neo-formed fault scarps and drainage modification as proxies of present day tectonics at the Abu Dabbab area, Eastern Desert, Egypt. Assiut. Univ. J. Geol. 37 (2), 25–63.

Aki, K., 1965. Maximum likelihood estimate of *b* in the formula log $N = a - bM$ and its confidence limits. Bull. Earthq. Res. Inst. Tokyo Univ. 43, 237–239.

Badawy, A., El-Hady, Sh., Abdel-Fattah, Ak., 2008. Microearthquakes and neotectonics of Abu Dabbab, Eastern desert of Egypt. Seismol. Res. Lett. 79 (1), 55–67.

Bender, B., 1983. Maximum likelihood estimates of *b*-values for magnitude grouped data. Bull. Seismol. Soc. Am. 73, 831–851.

Bosworth, W., Strecker, M., 1997. Stress field changes in the Afro-Arabian rift systems during the Miocene to recent period. Tectonophysics 278, 47–62.

Cao, A., Gao, S.S., 2002. Temporal variation of seismic *b*-values beneath northeastern Japan island arc. Geophys. Res. Lett. 29 (9), 1334.

Daggett, P.H., Morgan, P., 1977. Egypt and the northern Red Sea: new microearthquake data. Trans. Am. Geophys. Union 58, 1198.

Daggett, P.H., Morgan, P., Boulos, F.K., Hennin, S.F., El-Sherif, A. A., El-Sayed, A.A., Basta, N.Z., Melek, Y.S., 1986. Seismicity and active tectonics of the Egyptian Red Sea margin and the northern Red Sea. Tectonophysics 125, 313–324.

Davis, K., Burbank, D.W., Fisher, D., Wallace, S., Nobes, D., 2005. Thrust-fault growth and segment linkage in the active Ostler fault zone, New Zealand. J. Struct. Geol. 27, 1528–1546.

El Gaby, S., List, F., Tehrani, R., 1988. Geology, evolution and metallogenesis of the Pan-African belt in Egypt. In: El Gaby, S., Greiling, R.O. (Eds.), The Pan-African belt of Northeast Africa and Adjacent Areas. Braunschweig, Vieweg, pp. 17–68.

El-Hady, S.M., 1993. Geothermal Evolution of the Red Sea Margin and Its Relation to Earthquake Activity Master's thesis. Cairo University, Cairo, Egypt.

Fairhead, J.D., Girdler, R.W., 1970. The seismicity of the Red Sea, Gulf of Aden and Afar triangle. Philos. Trans. Roy. Soc. A 267, 49–74.

Farrell, J., Smith, R.B., Taira, T., Puskas, C.M., Burlacu, R., Pechmann, J., Heasler, H., Lowenstern, J., 2009. Source properties and deformation analysis of the 2008–2009 Yellowstone Lake earthquake swarm. Seismol. Res. Lett. 80 (2), 339.

Gaulier, J.M., Le Pichon, X., Lyberis, N., Avedik, F., Geli, L., Moretti, I., Deschamps, A., Salah, Hafez., 1988. Seismic study of the crustal thickness of the northern Red Sea and Gulf of Suez. Tectonophysics 153, 55–88.

Gillespie, P.A., Walsh, J.J., Watterson, J., 1992. Limitations of dimension and displacement data from single faults and the consequences for data analysis and interpretation. J. Struct. Geol. 14, 1157–1172.

Gutenberg, R., Richter, C.F., 1944. Frequency of earthquakes in California. Bull. Seismol. Soc. Am. 34, 185–188.

Hamada, K., 1968. Ultra micro-earthquakes in the area around Matsushiro. Bull. Earthq. Res. Inst. 46, 271–318.

Hamilton, R.M., 1967. Mean magnitude of an earthquake sequence. Bull. Seismol. Soc. Am. 57, 1115–1116.

Hill, D.P., 1977. A model for earthquake swarms. J. Geophys. Res. 82, 1347–1352.

Hosny, A., El Hady, S.M., Mohamed, A.A., Panza, G.F., Tealeb, A., El Rahman, M.A., 2009. In: Magma Intrusion in the Upper Crust of Abu Dabbab Area, Southeast of Egypt, from Vp and Vp/Vs Tomography, vol. 20. Rendiconti Lincei, pp. 1–19. http://dx.doi.org/10.1007/s12210-009-0001-8.

Hosny, A., El Hady, Sh.M., Guidarelli, M., Panza, G.F., 2011. Source Moment Tensors of the Earthquake Swarm in Abu-Dabbab area. Rendiconti Lincei, South-East Egypt.

Hussein, H.M., Hurukawa, N., Al-Arifi, N.S., 2008. Relocation of Microearthquakes in Abu Dabaab region, Egypt using Modified Joint Hypocenter Determination Method. Individual Study. International Institute of Seismology and Earthquake Engineering, Tsukuba, Japan.

Hussein, H.M., Moustafa, S.S.R., Elawadi, E., Al-Arifi, N.S., Hurukawa, N., 2011. Seismological Aspects of the Abou Dabbab Region, Eastern Desert, Egypt. Seismol. Res. Lett. 82 (1).

Khodayar, M., Einarsson, P., 2004. Reverse slip structures at oceanic diverging plate boundaries and their Kinematic origin, data from Tertiary crust of west and south Iceland. J. Struct. Geol. 26 (11), 1945–1960.

Ibrahim, M.E., Yokoyama, I., 1994. Probable origin of Abu Dabbab earthquakes swarms in the Eastern Desert of Egypt. Bull. IISEE 32 (1998).

Ishimoto, M., Iida, K., 1939. Observations of earthquakes registered with the microseismograph constructed recently. Bull. Earthq. Res. Inst. 17, 443–478.

Marzouk, I., 1988. Study of the Crustal Structure of Egypt Deduced from Deep Seismic and Gravity Data. PhD Diss. Hamburg University, Hamburg, Germany.

Minakami, T., 1990. Prediction of volcanic eruptions. In: Civetta, L., Gasparini, P., Luongo, G., Rapolla, A. (Eds.), Physical Volcanology Elsevier, Amsterdam, pp. 1–27.

Mogi, K., 1962. Magnitude-frequency relations for elastic shocks accompanying fractures of various materials and some related problems in earthquakes. Bull. Earthq. Res. Inst. 40, 831–853.

Mohamed, G.A., 2005. A Detailed Microearthquakes Study at Abu Dabbab Area, Eastern Desert, Egypt Unpublished M.Sc. South Valley University, Egypt, p. 142.

Morgan, P., Keller, G.R., Boulos, F.K., 1981. Earthquake cannons in the Egyptian Eastern Desert. Bull. Seismol. Soc. Am 71, 551–554.

Scholz, C.H., 1968. The frequency-magnitude relation of microfracturing in rock and its relation to earthquakes. Bull. Seismol. Soc. Am. 58, 399–415.

Shi, Y., Bolt, B.A., 1982. The standard error of the Magnitude-frequency *b*-values. Bull. Seismol. Soc. Am. 72, 1677–1687.

Schorlemmer, D., Neri, G., Wiemer, S., Mostaccio, A., 2003. Stability and significance tests for *b*-value anomalies: example from the Tyrrhenian Sea. Geophys. Res. Lett. 30 (16), 1835. http://dx.doi.org/10.1029/2003GL017335.

Schorlemmer, D., Wiemer, S., Wyss, M., 2005. Variations in earthquake-size distribution across different stress regimes. Nature 437, 539–542.

Toda, Shinji, Stein, R.S., Sagiya, T., 2002. Evidence from the AD 2000 Izu Islands.

Utsu, T., 1999. Representation and analysis of the earthquake size distribution: a historical review and some new approaches. Pageoph 155, 509–535.

Vidale, J.E., Shearer, P.M., 2006. A survey of 71 earthquake bursts across southern California: exploring the role of pore fluid pressure fluctuations and aseismic slip as drivers. J. Geophys. Res. 111, B05312.

Waite, G.P., Smith, R.B., 2002. Seismic evidence for fluid migration accompanying Yellowstone Lake earthquake swarm. Seismol. Res. Lett. 80 (2), 339.

Warren, N.W., Latham, G.V., 1970. An experimental study of thermally induced microfracturing and its relation to volcanic seismicity. J. Geophys. Res. 75, 4455–4464.

Wiemer, S.A., 2001. Software package to analyze seismicity: ZMAP. Seismol. Res. Lett. 72, 373–382.

Wiemer, S., Katsumata, K., 1999. Spatial variability of seismicity parameters in aftershock zones. J. Geophys. Res. 104, 13135–13151.

Wiemer, S., McNutt, S.R., 1997. Variations in the frequency-magnitude distribution with depth in two volcanic areas: Mount St. Helens, Washington, and Mt. Spurr, Alaska. Geophys. Res. Lett. 24, 189–192.

Wiemer, S., Wyss, M., 1997. Mapping the frequency-magnitude distribution in asperities: an improved technique to calculate recurrence times. J. Geophys. Res. 102, 15115–15128.

Wiemer, S., Wyss, M., 2000. Minimum magnitude of completeness in earthquake catalogs: examples from Alaska, the western US and Japan. Bull. Seismol. Soc. Am. 90, 859–869.

Wyss, M., 1973. Towards a physical understanding of the earthquake frequency distribution. Geophys. J. Roy. Astron. Soc. 31, 341–359.

Wyss, M., Wiemer, S., 1997. Two current seismic quiescences within 40 km of Tokyo. Geophys. J. Int. 128, 459–473.

Wyss, M., Hasegawa, A., Wiemer, S., Umin, N., 1999. Quantitative mapping of precursory seismic quiescence before the 1989, M 7.1, off-Sanriku earthquake, Japan. Annali di Geophysica 42, 851–869.